

Europium Palladium Hydrides<sup>‡</sup>H. Kohlmann,<sup>\*,†</sup> H. E. Fischer,<sup>§,||</sup> and K. Yvon<sup>†</sup>

Laboratoire de Cristallographie, Université de Genève, 24 Quai Ernest Ansermet, CH-1211 Genève 4, Switzerland, and Institut Laue-Langevin, Avenue des Martyrs, BP 156X, F-38042 Grenoble Cedex, France

Received November 6, 2000

The first fully structurally characterized ternary europium palladium hydrides (deuterides) are reported. The most Eu rich compound is Eu<sub>2</sub>PdD<sub>4</sub>. Its  $\beta$ -K<sub>2</sub>SO<sub>4</sub> type structure (space group *Pnma*,  $a = 749.47(1)$  pm,  $b = 543.34(1)$  pm,  $c = 947.91(1)$  pm,  $Z = 4$ ) contains tetrahedral 18-electron [PdD<sub>4</sub>]<sup>4-</sup> complex anions and divalent Eu cations. The compound is presumably nonmetallic and shows paramagnetic behavior ( $\mu_{\text{eff}} = 8.0(2) \mu_{\text{B}}$ ) with ferromagnetic ordering at  $T_{\text{C}} = 15.1(4)$  K. A metallic compound at intermediate Eu content is EuPdD<sub>3</sub>. It crystallizes with the cubic perovskite structure (space group *Pm3m*,  $a = 380.01(2)$  pm,  $Z = 1$ ) in which palladium is octahedrally surrounded by fully occupied deuterium sites. Metallic hydrides at low Eu content form by reversible hydrogen absorption of intermetallic EuPd<sub>2</sub> (*Fd3m*,  $a = 775.91(1)$  pm,  $Z = 8$ ). Depending on the experimental conditions at least three phases with distinctly different hydrogen contents  $x$  exist: EuPd<sub>2</sub>H <sub>$x \approx 0.1$</sub>  ( $a = 777.02(2)$  pm,  $Z = 8$ ,  $T = 298$  K,  $p(\text{H}_2) = 590$  kPa), EuPd<sub>2</sub>H <sub>$x \approx 1.5$</sub>  ( $a = 794.47(5)$  pm,  $Z = 8$ ,  $T = 298$  K,  $p(\text{H}_2) = 590$  kPa), and EuPd<sub>2</sub>H <sub>$x \approx 2.1$</sub>  ( $a = 802.1(1)$  pm,  $Z = 8$ ,  $T = 350$  K,  $p(\text{H}_2) = 610$  kPa). All crystallize with cubic Laves phase derivative structures and have presumably disordered hydrogen distributions.

## 1. Introduction

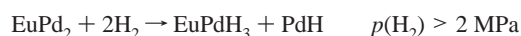
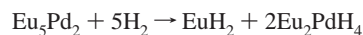
Ternary metal hydrides are of interest for hydrogen storage applications.<sup>1</sup> Systems based on europium are only rarely investigated because of the high costs of synthesis and the difficulties associated with their structural characterization.<sup>2–4</sup> A system of particular interest from a crystal chemistry point of view is the ternary Eu–Pd–H system because the binary metal hydrides have rather different bonding types, i.e., EuH<sub>2</sub> is salt-like and stoichiometric while PdH <sub>$x$</sub>  is metallic and nonstoichiometric. These properties presumably change gradually as one replaces progressively one metal by the other. The only ternary phase known in that system is EuPdH<sub>2.9</sub>,<sup>5</sup> whose structure and composition, however, have not been fully characterized. In this paper we investigate that compound in more detail and give evidence for at least two more ternary hydride phases for which structures and magnetic data are presented.

Europium-containing hydrides are difficult to characterize from a structural point of view because of the strong absorption cross section of natural europium for thermal neutrons.<sup>6</sup> Recently, however, it was shown that useful data can be obtained

for such hydrides by tuning the neutron wavelength close to the minimum of the neutron absorption cross section of natural europium, and by using annular sample holders on high-intensity neutron diffractometers. This resulted in the successful characterization of the ionic hydrides EuH<sub>2</sub>, EuLiH<sub>3</sub>, EuMgH<sub>4</sub>, and EuMg<sub>2</sub>H<sub>6</sub>.<sup>2,3</sup>

## 2. Experimental Section

**2.1. Synthesis.** The starting materials were ingots of europium in the natural isotopic mixture, <sup>151</sup>Eu (Arris International, 99.9%), palladium foil (Strem Chemicals, 99.9%), palladium powder (Strem Chemicals, 99.9%), and hydrogen (Carbagas, 99.9999%) and deuterium gas (AGA, 99.8%). All materials were handled in an argon-filled glovebox. EuH<sub>2</sub> and EuD<sub>2</sub> were prepared according to ref 3. For the syntheses of ternary hydrides two routes were used: reaction of EuH<sub>2</sub> with palladium powder in hydrogen atmosphere up to 10 MPa at temperatures up to 750 K, and hydrogenation of intermetallic europium palladium compounds or alloys. Similar results were obtained by both techniques, but the second route provided better crystallized samples, higher yields, and fewer byproducts than the first route. The alloy “Eu<sub>2</sub>Pd” and the intermetallic compounds Eu<sub>3</sub>Pd<sub>2</sub>, Eu<sub>3</sub>Pd<sub>2</sub>, EuPd, and EuPd<sub>2</sub> were prepared by arc melting europium ingots and palladium foil in an argon atmosphere. Hydrogenation was carried out in an autoclave at hydrogen pressures up to 10 MPa and temperatures up to 750 K. The reactions could be formulated as



(6) Sears, V. F. *Neutron News* 1992, 3, 26–37.

\* Corresponding author: kohlmann@physics.unlv.edu, fax [+1] (702) 895 0804. New address: High Pressure Science and Engineering Center, Department of Physics, 4505 Maryland Parkway, Box 4002, University of Nevada, Las Vegas, NV 89154-4002.

<sup>‡</sup> Dedicated to Professor Horst P. Beck on the occasion of his 60th birthday.

<sup>†</sup> Université de Genève.

<sup>§</sup> Institut Laue-Langevin.

<sup>||</sup> New address: LURE, Batiment 209d, Centre Universitaire Paris-Sud, B.P. 34, 91898 Orsay Cedex, France.

(1) For a recent review, see: Sastri, M. V. C.; Viswanathan, B.; Srinivasa Murthy, S. *Metal Hydrides*; Narosa Publishing House: New Dehli, 1998.

(2) Kohlmann, H.; Gingl, F.; Hansen, T.; Yvon, K. *Angew. Chem., Int. Ed.* 1999, 38, 2029–2032.

(3) Kohlmann, H.; Yvon, K. *J. Alloys Compd.* 2000, 299, L16–L20.

(4) Kohlmann, H. *Physica B* 2000, 276–278, 288–289.

(5) Buschow, K. H. J.; Cohen, R. L.; West, K. W. *J. Appl. Phys.* 1977, 48, 5289–5295.

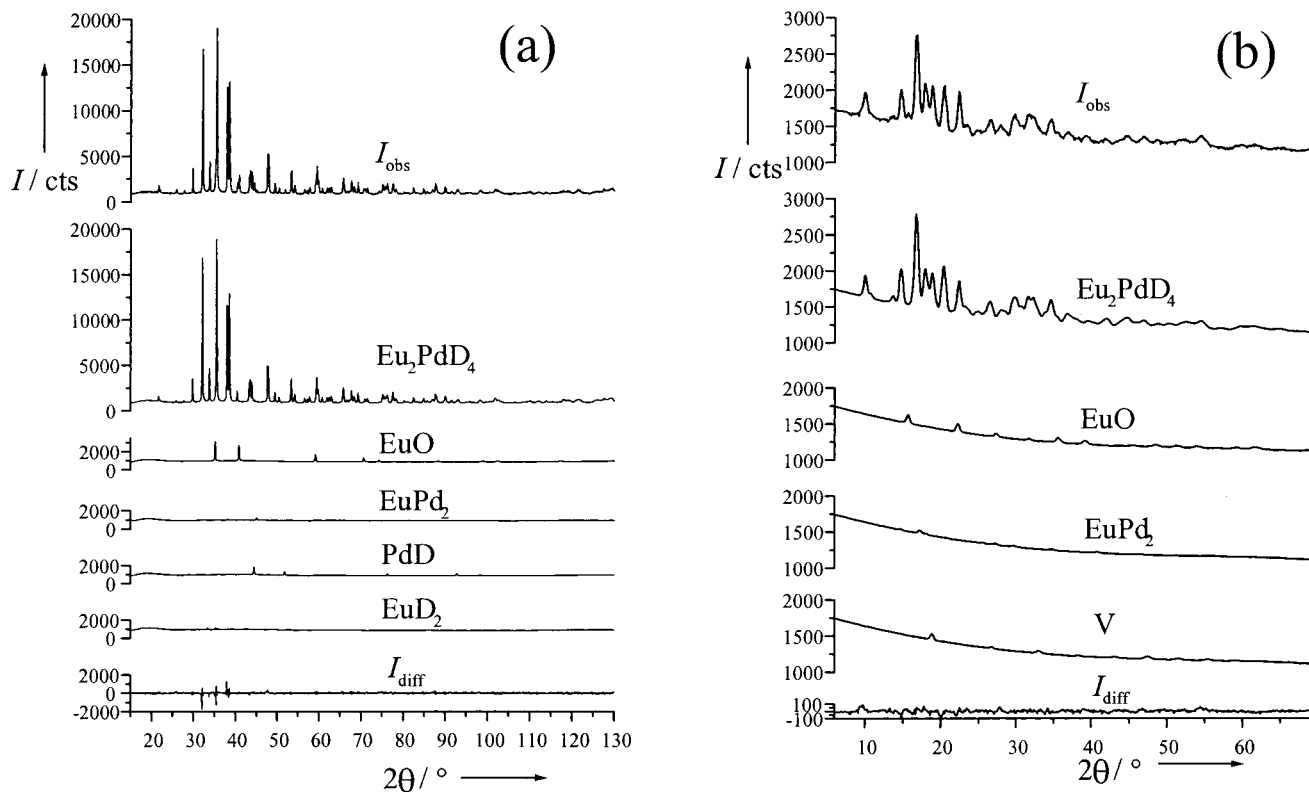


**Figure 1.** (a) Observed (top), calculated (middle), and difference (bottom) X-ray powder diffraction patterns of the  $\text{Eu}_2\text{PdD}_4$  sample ( $T = 293$  K, Co  $K\alpha$  radiation). All calculated patterns contain the refined background. Intensity in total detector counts. (b) Observed (top), calculated (middle), and difference (bottom) neutron powder diffraction patterns of the  $\text{Eu}_2\text{PdD}_4$  sample ( $T = 293$  K,  $\lambda = 70.51$  pm). Vanadium reflections are due to diffraction from the sample holder. All calculated patterns contain the refined background. The background is sloped because of the paramagnetic contribution to the scattering for the neutron case. Intensity in total detector counts.

and were checked by X-ray powder diffraction and gravimetric analysis.  $\text{EuPdH}_3$  ( $\text{EuPdD}_3$ ) was obtained as a fine black powder after hydrogenation (deuteration) of intermetallic  $\text{EuPd}$  at  $T = 500$  K and 1.5 MPa hydrogen (deuterium) pressure during 10 days. The weight uptake of the deuteride suggested the composition  $\text{EuPdD}_{2.95(5)}$ .  $\text{Eu}_2\text{PdH}_4$  ( $\text{Eu}_2\text{PdD}_4$ ) was prepared from the “ $\text{Eu}_2\text{Pd}$ ” alloy at  $T = 600$  K and 4.8 MPa hydrogen (deuterium) pressure during 10 days. The reaction products were annealed at  $T = 750$  K and 6.5 MPa hydrogen (deuterium) pressure for 3 days, and appeared as dark gray powders with a faint violet luster. The weight uptake of the deuteride suggested the composition  $\text{Eu}_2\text{PdD}_{4.26(3)}$ . The deviation from the stoichiometric formula  $\text{Eu}_2\text{PdD}_4$  was attributed to the formation of small amounts of  $\text{EuO}$  during synthesis.  $\text{Eu}_2\text{PdH}_4$  and  $\text{EuPdH}_3$  could be kept in air for a few days without decomposing, while  $\text{EuPd}_2\text{H}_x$  quickly releases hydrogen in air.

**2.2. X-ray Diffraction.** Diffraction data on  $\text{Eu}_2\text{PdH}_4$  and  $\text{Eu}_2\text{PdD}_4$  were collected on an OMNI powder diffractometer with Bragg–Brentano geometry (Co  $K\alpha$  radiation, data range  $15^\circ \leq 2\theta \leq 130^\circ$ , step size  $\Delta 2\theta = 0.03^\circ$ , total data collection time 21.3 h, Figure 1a). Data on  $\text{EuPdH}_3$  were obtained by the Guinier film technique (Co  $K\alpha$  radiation) on samples enclosed in sealed glass capillaries of 0.3 mm outer diameter. Data on the hydrides of  $\text{EuPd}_2$  were obtained by in situ measurements at hydrogen pressures around 600 kPa and temperatures between 290 and 750 K in a PAAR reaction chamber as mounted on a Bragg–Brentano diffractometer (Philips PW1820, Cu  $K\alpha$  radiation, data range  $15^\circ \leq 2\theta \leq 70^\circ$ , step size  $\Delta 2\theta = 0.03^\circ$ , counting time 10 s/step). In a first step data were taken on  $\text{EuPd}_2$  in a vacuum. In a second step the reaction chamber was filled with 600 kPa of hydrogen (Carbagas, 99.999%) and diffraction data were collected at the following temperatures and hydrogen pressures: 298 K (590 kPa), 350 K (610 kPa), 400 K (620 kPa), 298 K (510 kPa) (Figure 2). Data collection at each step started after the hydrogen pressure remained constant for a few hours, which ensured that the hydrogen absorption or desorption reaction was finished.

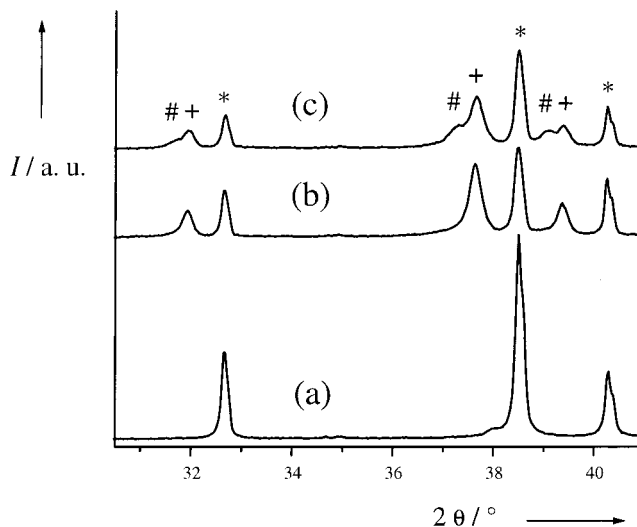


**Figure 2.** In situ X-ray powder diffraction patterns of the hydrogenation of the cubic Laves phase  $\text{EuPd}_2$  (section  $30.5^\circ \leq 2\theta \leq 41^\circ$ ). (a)  $\text{EuPd}_2$  at room temperature in a vacuum ( $a = 775.91(1)$  pm); the weak additional reflection at  $2\theta = 38^\circ$  is due to a PdH impurity. (b) Room temperature,  $p(\text{H}_2) = 590$  kPa,  $\text{EuPd}_2\text{H}_{\approx 0.1}$  with  $a = 777.02(2)$  pm,  $\text{EuPd}_2\text{H}_{\approx 1.5}$  with  $a = 794.47(5)$  pm. (c)  $T = 350$  K,  $p(\text{H}_2) = 610$  kPa,  $\text{EuPd}_2\text{H}_{\approx 0.1}$  (marked \*) with  $a = 777.35(2)$  pm,  $\text{EuPd}_2\text{H}_{\approx 1.5}$  (marked +) with  $a = 794.65(5)$  pm,  $\text{EuPd}_2\text{H}_{\approx 2.1}$  (marked #) with  $a = 802.1(1)$  pm. For all phases the patterns are consistent with a cubic Laves phase type metal host structure (C15,  $\text{MgCu}_2$  type). Lattice parameters were refined using the whole data range  $15^\circ \leq 2\theta \leq 70^\circ$ .

**2.3. Neutron Diffraction.** Powder diffraction data were collected for the deuterides  $\text{Eu}_2\text{PdD}_4$  (2.3 g) and  $\text{EuPdD}_3$  (1.8 g) on the high-intensity–short-wavelength neutron diffractometer D4b at the Institut

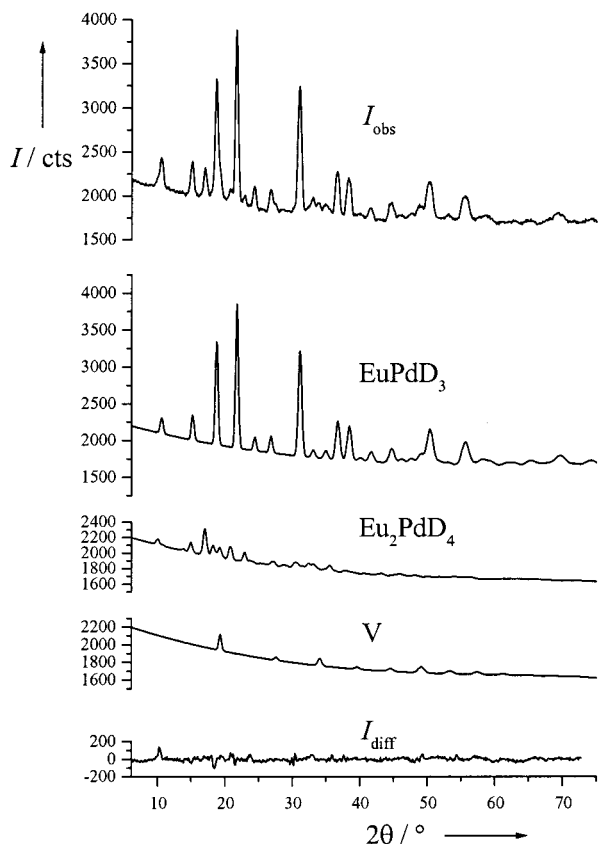


**Figure 3.** Observed (top), calculated (middle), and difference (bottom) neutron powder diffraction patterns of the  $\text{EuPd}_3$  sample ( $T = 293$  K,  $\lambda = 70.50$  pm). Vanadium reflections are due to diffraction from the sample holder. All calculated patterns contain the refined background. The background is sloped because of the paramagnetic contribution to the scattering. Intensity in total detector counts.

Laue-Langevin (Grenoble, France). In order to reduce the severe absorption a wavelength close to the minimum of the neutron absorption cross section,  $\sigma_a$ , of  $^{151}\text{Eu}$  ( $\sigma_a(^{151}\text{Eu}) = 860$  b (barn) at  $\lambda = 72.9$  pm $^4$ ) was chosen, and the samples were filled into double-walled vanadium cylinders (64 mm length, 9.15 mm inner diameter of the outer tube, annular sample thickness 0.6 mm, hermetically sealed by an indium wire). While the D4b diffractometer was fully operational for the measurements on  $\text{EuPd}_3$ , a failure of the hot source during the measurements on  $\text{Eu}_2\text{Pd}_4$  reduced the neutron flux at the wavelength chosen by about 70%. In this context it is worth pointing out that despite the optimized experimental conditions the neutron absorption in the samples investigated was still rather high (calculated linear absorption coefficients  $\mu = 17.76$  cm $^{-1}$  for  $\text{Eu}_2\text{Pd}_4$  and  $15.71$  cm $^{-1}$  for  $\text{EuPd}_3$  at  $\lambda = 70$  pm) and influenced adversely the quality of the data (Figures 1 and 3). Thus the accuracy of the structural results can not be expected to reach the standard of usual structure determinations. Precise values of wavelengths (zeroshifts) were determined from measurements of a standard nickel sample and found to be  $70.647(8)$  pm ( $-0.1713(2)^\circ$ ) and  $70.50(1)$  pm ( $-0.214(4)^\circ$ ) for  $\text{Eu}_2\text{Pd}_4$  and  $\text{EuPd}_3$ , respectively. The data were collected at room temperature beginning at  $2\theta = 3^\circ$  and  $6^\circ$  (step size  $1.9^\circ$ , data point spacing  $0.1^\circ$ ) during a total collection time of 20.5 and 6 h for  $\text{Eu}_2\text{Pd}_4$  and  $\text{EuPd}_3$ , respectively. In view of the relatively low resolution of the high-angle data, only data of the first detector (in the range  $3^\circ \leq 2\theta \leq 70^\circ$ ) were used in the structure refinements (FullProf $^7$ ). The patterns are shown in Figures 1 and 3.

**2.4. Magnetic Susceptibility Measurements.**  $\text{Eu}_2\text{Pd}_4$  powder was pressed into a pellet (11.4 mg), placed in a nonmagnetic plastic sample holder and measured with a Quantum Design SQUID magnetometer. Magnetization data were recorded at fields of  $B = 0.01$  T in the

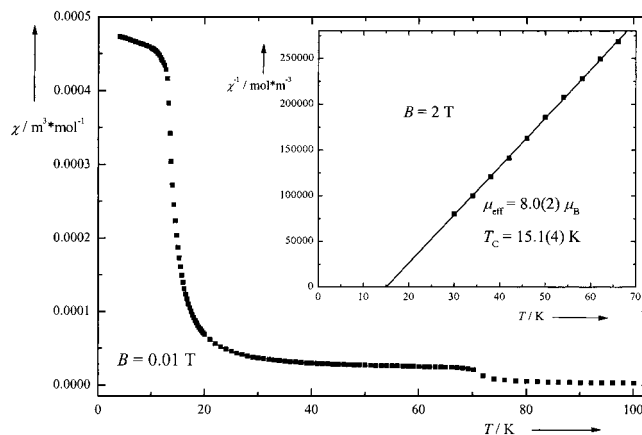


**Figure 4.** Magnetic susceptibility  $\chi$  of  $\text{Eu}_2\text{Pd}_4$  in the temperature range  $4$  K  $\leq T \leq 300$  K at  $B = 0.01$  T. Around  $T = 70$  K the ferromagnetic ordering of the byproduct  $\text{EuO}$  manifests itself as a kink in the curve. The data presented as a  $\chi^{-1}$  vs  $T$  plot ( $30$  K  $\leq T \leq 66$  K,  $B = 2$  T) in the inset are corrected for the ferromagnetic contribution of  $\text{EuO}$  (see text section 2.5).  $T_C$  and  $\mu_{\text{eff}}$  were calculated from the linear regression of the  $\chi^{-1}$  vs  $T$  plot.

temperature range  $4$  K  $\leq T \leq 100$  K, and  $B = 2$  T in the range  $30$  K  $\leq T \leq 300$  K. As shown in Figure 4 they display paramagnetic behavior with an onset of ferromagnetic ordering at  $15$  K. Below  $69.5$  K the  $\text{EuO}$  impurity orders ferromagnetically and gives a non-negligible contribution to the magnetization of the whole sample ( $\approx 10$ – $15\%$ ) as can be seen by the kink in the  $\chi$  vs  $T$  plot. This contribution was estimated from the temperature dependent saturation magnetization of  $\text{EuO}$  in the ferromagnetic state $^8$  and the mass fraction of  $\text{EuO}$  in the sample as determined by X-ray phase analysis, and then subtracted from the raw magnetization data in the range  $30$  K  $\leq T \leq 66$  K for the high-field measurement ( $B = 2$  T, see insert in Figure 4). From these data the Curie temperature  $T_C$  and the effective magnetic moment  $\mu_{\text{eff}}$  were calculated from a linear regression of the  $\chi^{-1}$  vs  $T$  plot (Figure 4, insert) in the paramagnetic state according to the Curie–Weiss law  $\chi^{-1} = (T - T_C)C^{-1}$  and  $\mu_{\text{eff}} = (3kCN_A^{-1}\mu_0^{-1}n^{-1})^{1/2}\mu_B^{-1}$  with  $k$  = Boltzmann's constant,  $C$  = Curie constant,  $N_A$  = Avogadro's constant,  $\mu_0$  = vacuum permeability,  $n$  = number of magnetic atoms per formula unit. The values found are  $T_C = 15.1(4)$  K and  $\mu_{\text{eff}} = 8.0(2)$   $\mu_B$ . The content of all byproducts (see below) was accounted for in the calculations. Estimated standard uncertainties of the results were determined by estimating the errors of all experimentally determined values.

### 3. Crystal Structure Determination

**3.1.  $\text{Eu}_2\text{PdH}_4$ .** The X-ray patterns of  $\text{Eu}_2\text{PdH}_4$  were indexed to an orthorhombic unit cell, and good agreement between observed and calculated patterns was obtained by assuming a  $\beta$ - $\text{K}_2\text{SO}_4$  type arrangement (space group  $Pnma$ ) with positional parameters as in  $\text{Sr}_2\text{PdH}_4$ . $^9$  Rietveld refinements (DBWS) $^{10}$  yielded the cell parameters  $a = 750.85(6)$  pm,  $b = 544.70(3)$  pm, and  $c = 959.85(7)$  pm for the hydride. The detailed structure refinements were carried out on the deuteride sample  $\text{Eu}_2\text{PdD}_4$  by using the same sample for X-ray and neutron diffraction. Metal atom positions were first refined on X-ray data and then held fixed during refinement of the deuterium positions on neutron data. The X-ray results indicated a small amount of  $\text{EuO}$  and traces of  $\text{EuPd}_2$ ,  $\text{PdD}$ , and  $\text{EuD}_2$  (Figure 1a). During the structure refinements the zero point and sample displacement were held constant at the values determined from a measurement

(8) McGuire, F. T. R.; Methfessel, S. In *Landolt-Börnstein, Numerical Data and Functional Relationships in Science and Technology*; New Series; Springer-Verlag: Berlin, 1970; Vol. III4a, p 74.

(9) Olofsson-Martenson, M.; Kritikos, M.; Noreus, D. *J. Am. Chem. Soc.* **1999**, *121*, 10908–10912.

(10) Young, R. A.; Sakthivel, A.; Moss, T. S.; Paiva-Santos, C. O. *J. Appl. Crystallogr.* **1995**, *28*, 366–367.

(7) Rodríguez-Carvajal, J. *FullProf*, Version 3.1d; LLB (unpublished), 1996.

**Table 1.** Crystal Structure Data of  $\text{Eu}_2\text{PdD}_4$  Refined from Neutron Powder Diffraction Data and X-ray Diffraction Powder Data (in Italics) Collected on the Same Sample<sup>a</sup>

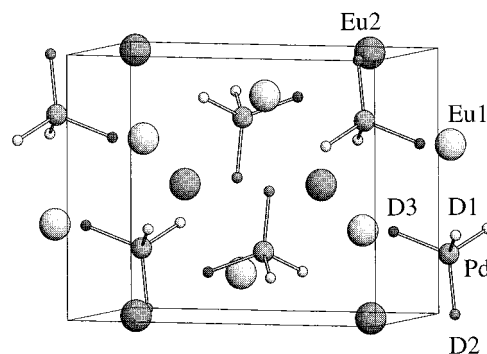
space group $Pnma$ (No. 62), $a = 749.47(1)$ pm, $b = 543.34(1)$ pm, $c = 957.91(1)$ pm						
	site	$x/a$	$y/b$	$z/c$	$B_{\text{iso}}/10^4 \text{ pm}^2$	
	Eu1	<i>4c</i>	<i>0.1513(3)</i>	<i>1/4</i>	<i>0.4082(3)</i>	3.1(3)
	Eu2	<i>4c</i>	<i>0.4901(2)</i>	<i>1/4</i>	<i>0.6703(2)</i>	1.8(2)
	Pd	<i>4c</i>	<i>0.2387(3)</i>	<i>1/4</i>	<i>0.0848(3)</i>	0.4(2)
	D1	<i>8d</i>	<i>0.324(1)</i>	<i>0.502(3)</i>	<i>0.159(1)</i>	1.5(2)
	D2	<i>4c</i>	<i>0.011(1)</i>	<i>1/4</i>	<i>0.104(1)</i>	1.8(3)
	D3	<i>4c</i>	<i>0.320(2)</i>	<i>1/4</i>	<i>0.905(1)</i>	0.9(2)
X-ray: <sup>b</sup>			$R_p = 3.5\%$ , $R_{\text{wp}} = 4.4\%$ , $S = 1.6$ , $R_{\text{Bragg}} = 5.0\%$			
neutron: <sup>b</sup>			$R_p = 6.0\%$ , $R_{\text{wp}} = 7.8\%$ , $S = 2.6$ , $R_{\text{Bragg}} = 3.5\%$			

<sup>a</sup> Structural parameters refined from X-ray data were held fixed in the refinements on neutron data. Form of the temperature factor:  $T = \exp[-B_{\text{iso}}(\sin \theta/\lambda)^2]$ . <sup>b</sup>  $R$  factors:  $R_p = \sum |y_i(\text{obs}) - y_i(\text{calc})| / \sum y_i(\text{obs})$ ;  $R_{\text{wp}} = [\sum w_i(y_i(\text{obs}) - y_i(\text{calc}))^2 / \sum w_i y_i(\text{obs})^2]^{1/2}$ ;  $R_{\text{Bragg}} = \sum |I_B(\text{obs}) - I_B(\text{calc})| / \sum I_B(\text{obs})$ .

of a silicon standard. The background was described by linear interpolation between 23 points, and the profiles were described by the pseudo-Voigt function. The following 38 parameters were allowed to vary in the final X-ray refinement: one scale factor, three lattice, three half-width, two mixing, one asymmetry, one preferred orientation, six positional, and three thermal displacement parameters (metal atoms only) for  $\text{Eu}_2\text{PdD}_4$ ; one scale factor, one lattice, three half-width, one mixing, and one overall thermal displacement parameter for  $\text{EuO}$ ; one scale factor, one lattice, one half-width, and one mixing parameter for each of  $\text{EuPd}_2$  and  $\text{PdD}$ ; and one scale factor, one half-width, and one mixing parameter for  $\text{EuD}_2$ . For  $\text{EuD}_2$  the structural parameters from ref 3 were used. The contribution of the deuterium atoms was neglected.

The neutron data confirmed the unit cell and space group. Good agreement between observed and calculated patterns was obtained by taking the deuterium atom positions from  $\text{Sr}_2\text{PdD}_4$ <sup>9</sup> as starting values, thus confirming the  $\beta\text{-K}_2\text{SO}_4$  type structure. During the refinements the following parameters were fixed: zero-point shift as refined from the nickel standard, positional parameters of metal atoms in  $\text{Eu}_2\text{PdD}_4$ , and lattice parameters of all phases refined from X-ray data (see above). The background was described by a polynomial of fourth order, and the line profiles were described by the pseudo-Voigt function. The following 29 parameters were varied in the final refinement on neutron data: one scale factor, seven positional (deuterium atoms only), six thermal displacement, three half-width, one mixing, and one asymmetry parameter for  $\text{Eu}_2\text{PdD}_4$ ; one scale factor and one overall thermal displacement parameter for  $\text{EuO}$ ; one scale factor for  $\text{EuPd}_2$ ; one scale factor and one lattice parameter for V (diffraction from sample holder); and five background parameters. The profile parameters of the minority phases and of vanadium were constrained to be equal to those of the main phase  $\text{Eu}_2\text{PdD}_4$ . These restrictions are justified as the peak widths are determined by the relatively low resolution of the instrument rather than by intrinsic properties of the sample. Results of the refinements and interatomic distances are summarized in Tables 1 and 3, respectively. Figures 1 and 5 show graphical representations of the refinements and the crystal structure of  $\text{Eu}_2\text{PdD}_4$ , respectively.

**3.2.  $\text{EuPdH}_3$ .** The X-ray patterns confirmed the CsCl type metal structure as proposed in ref 5 for  $\text{EuPdH}_{2.9}$ . The cell parameter of  $\text{EuPdH}_3$  was refined to  $a = 383.9(2)$  pm by a least-squares procedure from reflection positions on Guinier films as corrected by an internal standard silicon. The hydrogen

**Figure 5.** Crystal structure of  $\text{Eu}_2\text{PdD}_4$  ( $\beta\text{-K}_2\text{SO}_4$  type) viewed approximately along the crystallographic  $b$  axis. Covalent Pd–D bonds are drawn out. Note the distortion of the  $\text{PdD}_4$  polyhedron (point symmetry  $m$ ) with the elongated Pd–D3 bond.**Table 2.** Crystal Structure Data of  $\text{EuPdD}_3$  Refined from Neutron Powder Diffraction Data<sup>a</sup>

space group $Pm\bar{3}m$ (No. 221), $a = 380.01(2)$ pm						
	site	$x/a$	$y/b$	$z/c$	$B_{\text{iso}}/10^4 \text{ pm}^2$	
	Eu	<i>1b</i>	<i>1/2</i>	<i>1/2</i>	<i>1/2</i>	1.02(6)
	Pd	<i>1a</i>	0	0	0	0.02(7)
	D	<i>3d</i>	<i>1/2</i>	0	0	1.28(4)
						$R_p = 3.2\%$ , $R_{\text{wp}} = 4.8\%$ , $S = 2.6$ , $R_{\text{Bragg}} = 5.2\%$

<sup>a</sup> For the form of the temperature factor and definition of  $R$  factors, see Table 1.

**Table 3.** Selected Interatomic Distances (pm) and Bond Angles (deg) in  $\text{Eu}_2\text{PdD}_4$  and  $\text{EuPdD}_3$ 

$\text{Eu}_2\text{PdD}_4$					
Eu1–D2	270(1)	Eu2–2D1	254(1)	Pd–2D1	167(1)
Eu1–2D3	272.5(1)	Eu2–D3	258(2)	Pd–D2	172(1)
Eu1–2D1	276(1)	Eu2–D3	259(1)	Pd–D3	182(1)
Eu1–2D1	288(1)	Eu2–D2	263(1)		
Eu1–2D1	304(1)	Eu2–2D1	271(1)		
Eu1–D3	306(2)	Eu2–2D2	279.0(3)		
Eu1–D2	310(1)				
shortest D–D contact:		D1–D1	270(2)		
shortest Eu–Eu contact:		Eu1–Eu2	357.1(3)		
bond angles:		D1–Pd–D1	110(1)		
		D1–Pd–D2	110(1)		
		D1–Pd–D3	106(1)		
		D2–Pd–D3	116(1)		
$\text{EuPdD}_3$					
Eu–12D	268.71(1)	Pd–6D	190.00(1)	D–8D	268.71(1)
Eu–6Eu	380.01(2)				

positions were determined from the neutron data on the deuteride  $\text{EuPdD}_3$ , thus confirming the cubic perovskite type structure. A few supplementary diffraction peaks suggest the presence of small amounts of  $\text{Eu}_2\text{PdD}_4$  whose structural parameters were held fixed during the structure refinements. Reflection profiles were modeled using the pseudo-Voigt function, and the background was described by a polynomial of fourth order. The following 19 parameters were refined: one zero-point and five background polynomial parameters; one scale factor, one lattice, three thermal displacement, one peak shape, three half-width parameters for  $\text{EuPdD}_3$ ; one scale factor for  $\text{Eu}_2\text{PdD}_4$ ; and one scale factor, one thermal displacement, and one lattice parameter for vanadium (sample holder). The peak shape and the three half-width parameters of  $\text{Eu}_2\text{PdD}_4$  and of vanadium were constrained to be equal to those of the main phase  $\text{EuPdD}_3$ . Refinements of the occupancy factors did not result in values significantly different from 1.0; thus they were fixed at full occupancy. The value of the occupancy of the deuterium site,



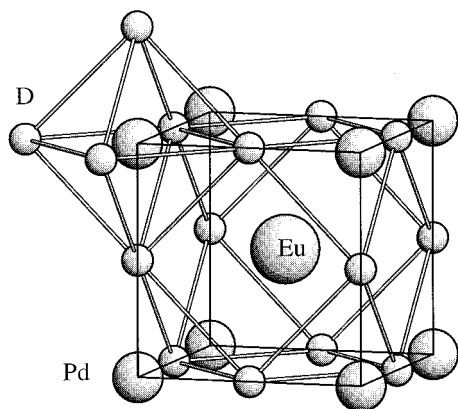


**Figure 6.** Crystal structure of  $\text{EuPd}_3$  (cubic perovskite type). Deuterium polyhedra around palladium (octahedron) and europium (cuboctahedron) are drawn out.

in particular, indicated the stoichiometry to be  $\text{EuPd}_{3.07(3)}$ . Refinements on absorption-corrected data (ABSOR)<sup>11</sup> did not yield significantly different results except for a small increase of the atomic displacement parameters. Refinement results and interatomic distances are listed in Tables 2 and 3, respectively. The observed and calculated neutron diffraction patterns are shown in Figure 3, and the crystal structure is depicted in Figure 6.

**3.3.  $\text{EuPd}_2\text{H}_x$  ( $x \approx 0.1, 1.5, 2.1$ ).** Binary  $\text{EuPd}_2$  was confirmed to crystallize with the cubic Laves phase type structure (C15,  $\text{MgCu}_2$  type),<sup>12</sup> and its lattice parameter was refined to  $a = 775.91(1)$  pm. Zero point and sample displacement were held constant at the values determined from a measurement of a silicon standard during the structure refinements of the  $\text{EuPd}_2$  sample before hydrogen exposure. For the data collected in situ during hydrogen exposure, the sample displacement parameter was refined to account for the volume expansion on hydrogenation and the thermal dilatation of the sample holder. For the structure refinements, data of the whole range  $15^\circ \leq 2\theta \leq 70^\circ$  were used. A small section of the patterns is shown in Figure 2. In situ X-ray diffraction showed that exposure to hydrogen at room temperature doubled the number of reflections such that the pattern could be resolved into two cubic patterns. One was almost identical to that of binary  $\text{EuPd}_2$  and had sharp reflections whereas the other was shifted toward higher  $d$  spacings and had broadened reflections (Figure 2b). Upon heating ( $T = 350$  K and  $p(\text{H}_2) = 610$  kPa) a third pattern appeared which was shifted toward still higher  $d$ 's (Figure 2c) and showed also broadened reflections. All patterns were consistent with expanded  $\text{EuPd}_2$  structures having refined lattice parameters of  $a = 777.02(2)$ ,  $794.47(5)$ , and  $802.1(1)$  pm. On the basis of the observation that cubic Laves phase hydrides usually undergo a volume expansion on the order of 5% per hydrogen atom per formula unit, the hydrogen content of the above hydride phases was estimated to be  $\text{EuPd}_2\text{H}_{\approx 0.1}$ ,  $\text{EuPd}_2\text{H}_{\approx 1.5}$ , and  $\text{EuPd}_2\text{H}_{\approx 2.1}$ , respectively. Hydrogen atoms were not located in the structure, but they are likely to occupy tetrahedral interstices. Further heating to  $T = 400$  K ( $p(\text{H}_2) = 620$  kPa) initiated decomposition into  $\text{EuPdH}_3$  and PdH.

#### 4. Discussion

$\text{Eu}_2\text{PdH}_4$  is a new ternary metal hydride that belongs to the class of so-called complex transition metal hydrides.<sup>13,14</sup> Its

$\beta\text{-K}_2\text{SO}_4$  type structure is built up by tetrahedral 18-electron  $[\text{Pd}^0\text{H}_4]^{4-}$  complex anions and  $\text{Eu}^{2+}$  cations. The hydrido complex is the first of that type known to be stabilized by europium. The compound is paramagnetic and orders ferromagnetically at about 15 K. The measured magnetic moment of  $8.0(2) \mu_B$  is in good agreement with the theoretical free ion value of  $7.95 \mu_B$  for  $\text{Eu}^{2+}$  (zero for  $\text{Eu}^{3+}$ ). Thus the compound can be safely described by the limiting ionic formula  $(\text{Eu}^{2+})_2 [\text{Pd}^0\text{H}_4]^{4-}$ . Palladium is formally zerovalent ( $d^{10}$ ) and has a presumably  $sp^3$  hybridized valence shell. While the D–Pd–D bond angles ( $106\text{--}116^\circ$ ) in the complex are close to the tetrahedral angle, the Pd–D bond distances show a relatively large spread ( $167\text{--}182$  pm, Figure 5, Table 3). Most other  $\beta\text{-K}_2\text{SO}_4$  type structures, including some deuterides, show smaller spreads of the tetrahedral bond distances, such as  $\beta\text{-K}_2\text{SO}_4$  ( $146\text{--}147$  pm),<sup>15</sup>  $\text{K}_2\text{CrO}_4$  ( $164\text{--}165$  pm),<sup>15</sup>  $\text{Rb}_2\text{ZnD}_4$  ( $166\text{--}168$  pm),<sup>16</sup>  $\text{Cs}_2\text{ZnD}_4$  ( $167\text{--}169$  pm),<sup>16</sup>  $\text{Rb}_2\text{MgD}_4$  ( $179\text{--}187$  pm),<sup>17</sup>  $\text{K}_2\text{ZnD}_4$  ( $163\text{--}167$  pm),<sup>18</sup>  $\text{Ba}_2\text{PdD}_4$  ( $178\text{--}181$  pm),<sup>9</sup> and  $\text{Sr}_2\text{PdD}_4$  ( $176\text{--}181$  pm).<sup>9</sup> The Pd–D bond distances within the series of known palladium-based deuterides ( $\text{Eu}_2\text{PdD}_4$ ,  $\text{Sr}_2\text{PdD}_4$ ,  $\text{Ba}_2\text{PdD}_4$ ) tend to increase as the size of the cation increases, which is presumably due to matrix effects. Shorter Pd–D bonds occur in  $\text{NaPd}_3\text{D}_2$  ( $183$  pm)<sup>19</sup> and in palladium hydrido complexes such as planar  $[\text{PdD}_4]^{2-}$  in  $\text{A}_3\text{PdD}_5$  ( $A = \text{K}, \text{Rb}, \text{Cs}$ ) and three-coordinated  $[\text{PdD}_3]^{3-}$  in  $\text{NaBaPdD}_3$ .<sup>20–22</sup> The structure of  $\text{Eu}_2\text{PdD}_4$  contains two Eu sites, one having 11-fold (Eu1) and the other 9-fold (Eu2) deuterium coordination. The 11-fold coordination is the first of that type found in europium-containing metal hydrides. As expected, the average Eu–D distance around the higher coordinated Eu1 ( $288$  pm) is longer than that around the lower coordinated Eu2 ( $265$  pm). This is also reflected by the atomic displacement parameters which are larger for Eu1 than for Eu2 (Table 1). Interestingly, the 11-fold coordinated Eu in  $\text{Eu}_2\text{PdD}_4$  has longer Eu–D distances than the 12-fold coordinated Eu in ionic  $\text{EuLiD}_3$  ( $268$  pm)<sup>3</sup> and metallic  $\text{EuPd}_3$  ( $269$  pm, Table 3). This is also true for nine-coordinated Eu2 that has longer Eu–D distances than in ionic deuterides having similar Eu coordinations such as  $\text{EuMgD}_4$  ( $252$  pm)<sup>2</sup> and  $\text{EuD}_2$  ( $255$  pm).<sup>3</sup>

$\text{EuPdH}_3$  is presumably identical to the cubic hydride phase  $\text{EuPdH}_{2.9}$  which has been described as a metallic conductor that contains divalent europium and orders ferromagnetically at 21 K.<sup>5,23</sup> According to the present work, that compound is stoichiometric, at least under the synthesis conditions chosen, and crystallizes with the cubic perovskite type structure (Table 2, Figures 3 and 6). Given that the cell parameter of the hydride  $\text{EuPdH}_3$  ( $a = 383.9(2)$  pm) is somewhat bigger than that reported for  $\text{EuPdH}_{2.9}$  ( $a = 380.6$  pm)<sup>5</sup> and that the former has been prepared at a higher hydrogen pressure than the latter, this compound may have a range of existence. Hydrogen deficiencies are known to occur in other cubic perovskite type hydrides such as  $\text{CaPdH}_2$  and  $\text{SrPdH}_{2.7}$ ,<sup>24</sup> and presumably also  $\text{YbPdH}_{2.7}$  and

- (14) Yvon, K. In *Encyclopedia of Inorganic Chemistry*; King, R. B., Ed.; Wiley: New York, 1994; Vol. 3, pp 1401–1420.
- (15) McGinney, J. A. *Acta Crystallogr., Sect. B: Struct. Sci.* **1972**, *28*, 2845–2852.
- (16) Bortz, M.; Hewat, A.; Yvon, K. *J. Alloys Comp.* **1997**, *248*, L1–L4.
- (17) Bortz, M.; Hewat, A.; Yvon, K. *J. Alloys Comp.* **1997**, *268*, 173–176.
- (18) Bortz, M.; Yvon, K.; Fischer, P. *J. Alloys Comp.* **1994**, *216*, 39–42.
- (19) Kadir, K.; Noreus, D. *Z. Phys. Chem.* **1993**, *179*, 249–253.
- (20) Bronger, W.; Auffermann, G. *J. Alloys Compd.* **1992**, *179*, 235–240.
- (21) W. Bronger, G. Auffermann, *J. Alloys Compd.* **1992**, *187*, 81–85.
- (22) Olofsson, M.; Kritikos, M.; Noreus, D. *Inorg. Chem.* **1998**, *37*, 2900–2902.
- (23) Orgaz, E.; Mazel, V.; Gupta, M. *Phys. Rev. B: Condens. Matter* **1996**, *54*, 16124–16130.

(11) Schmidt, D.; Ouladdiaf, B. *J. Appl. Crystallogr.* **1998**, *31*, 620–624.

(12) Iandelli, A.; Palenzona, A. *J. Less-Common Met.* **1974**, *38*, 1–7.

(13) Bronger, W. *Angew. Chem.* **1991**, *103*, 776–784.

$\text{YbNiH}_{2.7}$ .<sup>25</sup> Palladium in  $\text{EuPd}_3$  is octahedrally coordinated by deuterium at bond distances (190.00(1) pm, Table 3) that are intermediate between those found in covalent hydrides such as  $\text{Eu}_2\text{PdH}_4$  (167–182 pm) and metallic (interstitial) hydrides such as PdD (204 pm). Europium in  $\text{EuPd}_3$  has a cuboctahedral deuterium coordination with bond distances (268.71(1) pm) close to those in isotopic ionic  $\text{EuLiD}_3$  (267.82(2) pm).<sup>3</sup>

The cubic hydrides  $\text{EuPd}_2\text{H}_{\approx 0.1}$  and  $\text{EuPd}_2\text{H}_{\approx 1.5}$  derive from intermetallic  $\text{EuPd}_2$  by reversible hydrogen uptake at room temperature and 600 kPa hydrogen pressure. Both coexist even after long exposure to hydrogen, and they correspond to a solid solution ( $\alpha$ ) phase and a hydride ( $\beta$ ) phase, respectively. Upon heating to  $T = 350$  K, a third, more hydrogen rich cubic phase of composition  $\text{EuPd}_2\text{H}_{\approx 2.1}$  ( $\gamma$ -phase) forms. The latter decomposes at higher temperatures ( $T = 400$  K) and pressures into  $\text{EuPdH}_3$  and  $\text{PdH}_x$ . The hydrogen positions in all these phases have not been determined; however, in view of the structural analogy with other C15 type derivative hydrides,<sup>26</sup> it is likely that these atoms occupy tetrahedral interstices in the metal matrix. Thus, the phases  $\text{EuPd}_2\text{H}_x$  ( $x \approx 0.1, 1.5, 2.1$ ) are

(24) Bronger, W.; Ridder, G. *J. Alloys Compd.* **1994**, *210*, 53–55.

(25) Ensslen, K.; Bucher, E.; Oesterreicher, H. *J. Less-Common Met.* **1983**, *92*, 343–353.

(26) Yvon, K.; Fischer, P. In *Top. Appl. Phys. Vol. 63: Hydrogen in Intermetallic Compounds I*; Schlapbach, L., Ed.; Springer: Berlin, 1988; pp 87–138.

probably metallic interstitial hydrides having disordered hydrogen distributions.

## 5. Conclusion

The metal–hydrogen interactions in the Eu–Pd–H system show the following trends. At Eu rich compositions ( $\text{Eu}_2\text{PdH}_4$ ) the europium–hydrogen interactions are salt-like and involve exclusively divalent Eu as in binary  $\text{EuH}_2$  and other Eu-containing ionic metal hydrides,<sup>2,3</sup> while the palladium–hydrogen interactions are covalent. As the Pd content is increased ( $\text{EuPdH}_3$ ,  $\text{EuPd}_2\text{H}_x$ ), the bonding properties transform gradually and become metallic such as in binary  $\text{PdH}_x$ . The deuterium sites are fully occupied in  $\text{Eu}_2\text{PdD}_4$  and  $\text{EuPdD}_3$ , whereas in  $\text{EuPd}_2\text{H}_x$  hydrogen is probably disordered as in other typical interstitial, metallic hydrides. Thus europium palladium hydrides are another example for the versatility of hydrogen as a ligand for metals.

**Acknowledgment.** We gratefully acknowledge the help of Dr. Thomas Hansen, Dr. Gabriel Cuello, and Pierre Palleau (ILL, Grenoble, France) with the neutron diffraction experiments on D4b, and the help of Dr. Yuxing Wang (Institute of Condensed Matter Physics, University of Geneva, Switzerland) with the magnetic susceptibility measurements. This work was supported by the Swiss National Science Foundation.

IC001225D